Antiferromagnetic $LaFeO_3$ thin films and their effect on exchange bias

2008 J. Phys.: Condens. Matter 20 264014

(http://iopscience.iop.org/0953-8984/20/26/264014)

J. Phys.: Condens. Matter **20** (2008) 264014 (10pp) doi:10.1088/0953-8984/20/26/264014

Antiferromagnetic $LaFeO_3$ thin films and their effect on exchange bias

J W Seo[1], E E Fullerton[2], F Nolting[3], A Scholl[4], J Fompeyrine[5] and J-P Locquet[6]

[1] Department Metallurgy and Materials Engineering, Katholieke Universiteit Leuven, Kasteelpark Arenberg 44—bus 2450, B-3001 Heverlee, Belgium
[2] Center for Magnetic Recording Research CMRR and Department of Electrical and Computer Engineering, University of California San Diego, La Jolla, CA 92093-0401, USA
[3] Swiss Light Source, Paul Scherrer Institute, CH-5232 Villigen PSI, Switzerland
[4] Lawrence Berkeley National Laboratory, Berkeley, CA 94720, USA
[5] IBM Research Zurich GmbH, CH-8803 Rüschlikon, Switzerland
[6] Solid State Physics and Magnetism Section, Katholieke Universiteit Leuven, Celestijnenlaan 200d—bus 2414, B-3001 Heverlee, Belgium

E-mail: maria.seo@mtm.kuleven.be

Received 5 December 2007, in final form 20 May 2008
Published 9 June 2008
Online at stacks.iop.org/JPhysCM/20/264014

Abstract

Antiferromagnetic (AFM) orthoferrites are interesting model systems for exploring the correlation between their crystalline and AFM domains and the resulting exchange bias when coupled to a ferromagnetic layer. In particular, $LaFeO_3$ (LFO) has a Néel temperature, $T_N = 740$ K, which is the highest in the orthoferrite family. The recent developments of synchrotron radiation-based photoelectron emission microscopy (PEEM) have provided the possibility of studying AFM domain structures as well as the magnetic coupling between the AFM and the adjacent ferromagnetic (FM) layer, domain by domain. Thin films of LFO have proved excellent candidates for such studies because their AFM domains are well defined and large enough to be readily imaged by PEEM. This paper reviews the growth, structural and magnetic properties of LFO thin films as well as exchange coupling to a FM layer. The strong correlation between structural and AFM domains in this material allows us to investigate the exchange coupling as a function of the domain configuration, which can be changed by using different substrate material and substrate orientation. A significant increase of the exchange bias field by a factor of about 10 was obtained when LFO was diluted with Ni atoms in the volume part. In this sample, the structural domain boundary became corrugated due to substitutional defects. Our results indicate that the details of the precise domain boundary configuration strongly affect the exchange coupling.

(Some figures in this article are in colour only in the electronic version)

1. Introduction

Antiferromagnetic (AFM) materials are an essential element in magnetic devices, where they serve to pin the adjacent ferromagnetic (FM) reference layer into one preferred orientation. This coupling between the spins in the AFM and FM layers—called exchange bias—leads to a unidirectional anisotropy in the FM layer and induces a shift of the center of the FM hysteresis loop by a field H_{ex} (the exchange bias field) [1]. The biasing AFM layer is key component in the design of the sensor and determines to a large extent the long term stability. Although the exchange bias phenomenon has been known for more than five decades, fundamental aspects of the biasing mechanism itself are still controversial.

In AFM materials the magnetic moments are fully compensated due to AFM ordering of spins and do not respond to external magnetic fields. When the FM layer is brought into contact with the AFM layer the interfacial interaction produces a unidirectional anisotropy in the FM layer that depends on the thermal and field history of the

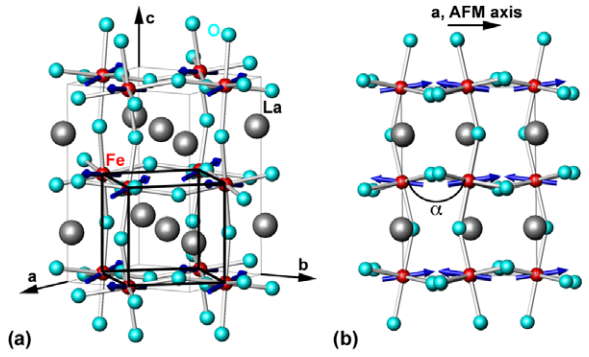

Figure 1. (a) Schematic drawing of the unit cell of LFO. The spins of Fe atoms (marked by small dark arrows) are oriented parallel to the a-axis of the orthorhombic unit cell. The perovskite unit cell drawn in black illustrates the epitaxial relationship. (b) (010) project of the unit cell. The buckling angle α is given by the Fe–O–Fe superexchange bonding.

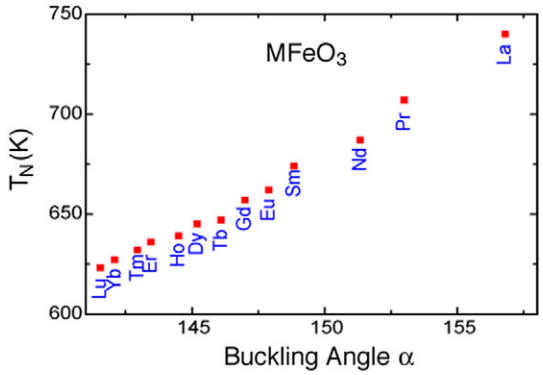

Figure 2. Néel temperature T_N of bulk orthoferrites is shown as a function of their buckling angle α. The data points are labeled with the M atoms of the orthoferrite $MFeO_3$. LFO (labeled by 'La') has the highest T_N and the largest α. Data extracted from [15, 16].

sample. To first order, if the AFM materials remain fully compensated at the interface then one might expect no net interaction between the FM and AFM layers. Thus, models explaining exchange bias phenomenon can mainly be divided into two categories: (i) models which assume perfect interface with uncompensated moments at the surface of the AFM layer [2] or (ii) models which suggest uncompensated moments at interface imperfections such as defects, grain or domains boundaries [3]. A number of experiments and theoretical models in the last years confirmed that exchange bias is correlated with the presence and morphology of AFM domains [4, 5] as well as the presence of uncompensated spins [6, 7]. In particular, with the breakthrough to image antiferromagnetic domains in $LaFeO_3$ (LFO) thin films by photo-emission electron microscopy (PEEM) [8] it became possible to investigate the direct magnetic coupling between the AFM and the adjacent FM layer [9]. These studies showed that the exchange coupling is given by one-to-one correlation of their magnetic domain structures and that the local bias varies with the domain size [10].

The orthoferrite LFO is an interesting AFM model system to explore the correlation between the domain structure and the resulting exchange bias. It has a Néel temperature, $T_N = 740$ K, which is the highest in the orthoferrite family. As shown in the schematic drawing (figure 1), the spins of the Fe atoms are aligned parallel to the a-axis of the orthorhombic crystal (space group $Pbnm$ with $a = 0.5557$ Å, $b = 0.55652$ Å and $c = 0.78542$ Å). The AFM alignment results from the superexchange coupling of the iron cations via the π orbitals of the oxygen atoms. The buckling of these Fe–O–Fe bonds to about 155° induces the orthorhombicity of the unit cell and is according to Lyubutin *et al* [11] responsible for the high Néel temperature. Indeed, as can be seen in figure 2 LFO contains the largest buckling angle in the orthoferrite family and exhibits the highest T_N. Owing to the large buckling angle, the orthorhombic structure can be identified on a local scale. Moreover, the direct correlation between the buckling angle and the superexchange coupling allows us to deduce the AFM axis from the structural orientation.

LFO can be grown epitaxially on perovskite or perovskite-like substrates, such as $SrTiO_3$ (STO), $LaAlO_3$ (LAO), MgO, and $MgAl_2O_4$ (MAO). As found by x-ray magnetic linear dichroism (XMLD) microscopy [8] and spectroscopy [12], thin films of LFO contain AFM domains, which are directly correlated with twin domains [13]. In the present paper we review the recent results on LFO. We also investigate the systematic modification of the domain structure and its effect on the exchange coupling.

2. Experimental details

Substrates of STO, LAO, MgO, and MAO are pre-annealed in vacuum for about one hour at 800 °C. The LFO films were grown in a molecular beam epitaxy (MBE) system using the block-by-block growth method [14] at 750 °C under a beam of atomic oxygen and a partial O_2 pressure of 5×10^{-6} Torr. For the growth of the diluted $LaNi_{0.1}Fe_{0.9}O_3$ (LNFO) in the volume part, the same growth condition was applied but 10% of Fe was replaced by Ni. Subsequent to the 20 nm thick diluted LNFO layer, a 1.2 nm thin LFO film was grown in order to preserve the same interface towards a subsequent magnetic layer. For magnetic measurements, an additional layer of Co or Fe was deposited on top of the LFO film after cooling to room temperature, followed by a 1 nm Pt protection layer.

The structural quality was monitored *in situ* by reflection high-energy electron diffraction (RHEED) and *ex situ* by x-ray diffraction (XRD) on a Siemens D500 diffractometer equipped with a graphite back monochromator. For the TEM study, plan-view and cross-sectional samples were prepared by grinding and thinning them with an Ar-ion beam to electron transparency. TEM studies were carried out with a 200 kV JEOL2010 and a 300 kV Philips CM300FEG microscope. The PEEM measurements were performed at the PEEM-2 microscope of the advanced light source mostly using Co as FM layer with a thickness of about 3 nm. The macroscopic magnetic characterization was performed with a Lakeshore vibrating sample magnetometer (VSM) and a Quantum Design superconducting quantum interference device (SQUID) magnetometer. With the former the magnetization was

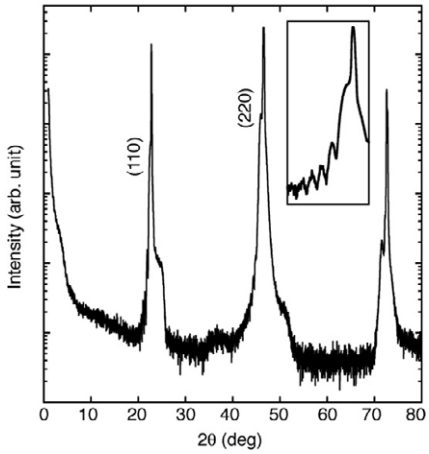

Figure 3. $\theta-2\theta$ x-ray diffractogram of a LFO film grown on (001) STO. The inset shows the low-angle finite-size oscillations around the (220) reflection.

Table 1. LFO was grown on various oxide substrates. For STO, two different orientations as well as vicinal substrates were used.

Substrates	Structure	Orientation hkl	d_{hkl} (Å)
$SrTiO_3$ (STO)	Cubic	(001)	3.905
		(110)	2.76
$LaAlO_3$ (LAO)	Pseudo-cubic	(001)	3.79
MgO	Cubic	(001)	4.21
$MgAl_2O_4$ (MAO)	Cubic	(001)	8.08

measured before and after annealing the samples in a 5000 Oe applied field for 15 min at 120 °C in ambient atmosphere. For SQUID measurements, the FM layer was typically 8 nm thick and the samples were annealed at 200 °C and 2000 Oe. The exchange bias field of Co/LFO, Fe/LFO and Co/LFO/LNFO films was determined from hysteresis loops measured by SQUID at temperatures between 10 and 350 K.

3. Growth of LFO thin films

Epitaxial films of LFO can be grown on perovskite substrates such as STO owing to their compatible structure and relatively small lattice mismatch. Table 1 summarizes the different substrate materials and orientation used in this study. As XRD analysis revealed, all LFO films grow epitaxially on the oxide substrates without any secondary phases. In general, at low 2θ angles finite-size oscillations were observed around the film diffraction peaks (figure 3), which allowed calculating the film thickness. For (001) STO, which is the most used substrate, an out-of-plane lattice parameter of $a = 3.947$ Å was derived. Compared with the bulk LFO lattice parameters, the out-of-plane lattice is expanded to about 0.4%.

During the growth, RHEED patterns were taken at different stages of the process. In figure 4(a), a RHEED pattern of (001) STO along the [100] azimuth is shown that was heated to 750 °C before deposition. The RHEED streaks are well defined—indicating a flat substrate surface—with a spacing of two streaks corresponding to STO. As LFO deposition starts, one additional streak instantaneously appears between two

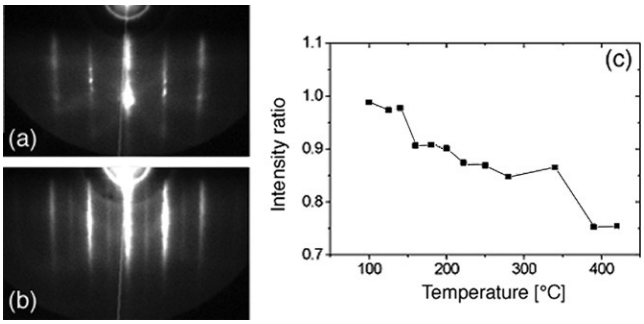

Figure 4. RHEED pattern taken (a) before growth and (b) after deposition of the first LFO unit cell. (c) shows the evolution of the relative intensity between the principal and the additional streaks as a function of the cooling temperature.

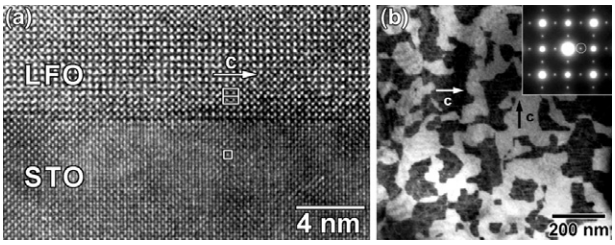

Figure 5. (a) Cross-sectional TEM image of LFO grown on (001) STO. The *c*-axis of the LFO orthorhombic unit cell is oriented parallel to the interface and to the [100] axis of STO. (b) Dark-field plan-view image of the LFO film obtained by selecting the superreflection marked by the circle in the diffraction pattern (inset). The four-fold symmetry of the diffraction pattern can be explained by the presence of the structural twins with the *c*-axis 90° rotated around the $[001]_{STO}$ zone axis.

principal streaks of STO (figure 4(b)). Its position corresponds to a doubling of the basic perovskite unit and suggests an alignment of the LFO *c*-axis parallel to the substrate surface from the very beginning of the film growth. An identical RHEED pattern was obtained when the substrate was rotated by 90° indicating a four-fold symmetry. This finding is, at first glance, not clear taking the orthorhombic structure of LFO into account but is correlated with the presence of structural twins which will be discussed later. The relative intensity of the additional streaks, which was obtained by calculating the intensity ratio between a main and an additional streak, was followed during and after the growth procedure. While the relative intensity remained almost constant during the growth, it increased linearly upon cooling to room temperature, as demonstrated in figure 4(c), suggesting an improved ordering along the *c*-axis.

4. Structural properties of LFO thin films

Typically LFO thin films grow epitaxially on perovskite substrates with an atomically sharp interface as the cross-sectional TEM image of LFO grown on (001) STO in figure 5 illustrates. In this image, the long *c*-axis of LFO is found to be indeed oriented in-plane and parallel to one of the perovskite principal axes in agreement with the RHEED observation. The

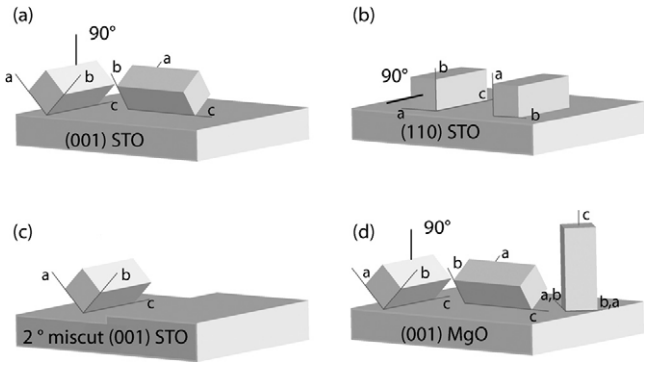

Figure 6. Schematic drawing of the twin configuration obtained on (a) (001) STO, (b) (110) STO, (c) 2° miscut (001) STO and (d) (001) MgO substrates. On the vicinal substrate, only the majority domain orientation is shown. In all samples, the *c*-axis preferentially lies on the substrate surface, except on MgO, where also domains with the *c*-axis perpendicular to the substrate surface are present.

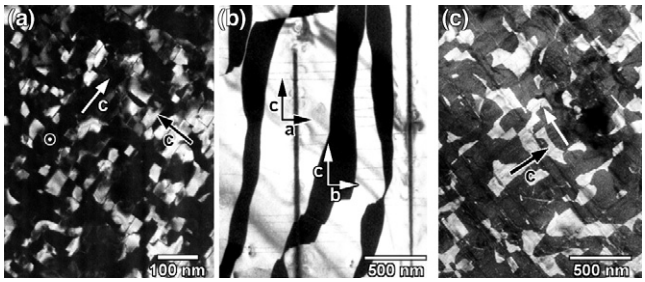

Figure 7. Dark-field TEM images of LFO thin films grown on (a) (001) MgO, (b) (110) STO and (c) 2° miscut (001) STO substrates.

epitaxial relationship between the film and (001) STO substrate can be described as follows: $(110)_{LFO} \parallel (001)_{STO}$ and $[001]_{LFO} \parallel [100]_{STO}$. Crystallographic twins have been found given by the 90° rotation of the *c*-axis around the substrate surface normal that corresponds to the [110] axis of LFO. As can be seen in the plan-view diffraction pattern (inset of figure 5(b)), the twin domains give rise to a diffraction pattern with a four-fold symmetry which originates from the overlap of two diffraction patterns in [110] zone but 90° rotated to each other. This phenomenon also explains the four-fold symmetry observed by RHEED. In plan-view TEM (figure 5(b)), the twin domains can be imaged in dark-field mode by selecting the respective superreflection correlated with the *c*-axis of LFO.

The shape and the size of the twin domains strongly depend on the orientation and the miscut angle of the substrate as well as on the film thickness [17]. However, which twin configuration is present depends on the substrate material. In figure 6 the relative crystallographic orientations are summarized for all applied substrates.

For STO and LAO substrates twin structures are comparable: on (001) substrates—which has been the orientation mostly investigated—the two domains with the *c*-axis oriented in-plane were obtained. Their typical size is about 200 nm for 8 nm thick LFO films. On (001) MgO and $MgAl_2O_4$ one additional domain type was found where the *c*-axis aligns out-of-plane. To be precise, these are two additional domain types because the (001) surface of MgO and MAO enables two equivalent (001) orientations where the *a*- and *b*-axes are exchanged by rotating the unit cell 90° around the *c*-axis. Since the difference between the *a*- and *b*-axis parameter is small (0.15%), and the crystalline symmetry is four-fold in these orientations, we cannot distinguish between both domain types. Therefore we refer to one domain type hereafter meaning both domain types with the *c*-axis out-of-plane. The domains are typically about 25 nm, hence significantly smaller compared to those on STO substrates. Figure 7(a) exhibits the structural twins in a TEM micrograph. The image was taken in plan-view dark-field mode by selecting one of the superreflections corresponding to the LFO orthorhombic *c*-axis. Each of the two domain types with the *c*-axis parallel to the substrate surface occupy about one third of the film surface. The residual one third of the domains has the *c*-axis parallel to the substrate normal as illustrated in the schematic drawing (figure 6(d)). In high-resolution TEM images, the latter domain type was found to be about three or four times smaller compared to its counterparts with the *c*-axis oriented in-plane [17].

The difference in domain size and domain configuration on STO and MgO substrates can be attributed to the larger lattice mismatch between LFO and MgO (7% instead of 0.58%) [13]. As domain walls can lead to strain relaxation, one expects more domains to be nucleated on MgO. Hence, more than ten times larger mismatch on MgO can qualitatively explain the much smaller domain size on MgO. Our previous atomic force microscopy studies also revealed a significantly higher surface roughness of the LFO grown on MgO indicating that the growth on MgO is three-dimensional [13].

On (110) STO, the *c*-axis remains in-plane, parallel to the [001] axis of STO, whereas the *a*- or the *b*-axis align parallel to the substrate normal. Hence, in this substrate orientation two domain types are formed by 90° rotation around the *c*-axis (figure 6(b)). The domain shape significantly changes to elongated stripe-like structures with about 200 nm in width and more than 2 μm in length (figure 7(b)). The long axis of the domain structures is aligned parallel to the *c*-axis of LFO. It has also to be noted that in addition to the above mentioned domain types 180° twins also occur, which originate from 180° rotation around the substrate surface normal. By TEM these twins are not distinguishable although they can yield different AFM axes and can be detected by XMLD spectroscopy [12].

When substrates with a miscut are used, domains with the *c*-axis perpendicular to the step edges get suppressed and those with the *c*-axis parallel to the step edges predominate. Figure 7(c) shows a dark-field TEM image of a LFO film grown on (001) STO substrate with a 2° miscut along one of the in-plane ⟨100⟩ directions. The fraction of the domains with the *c*-axis parallel to the step edges corresponds to about 80%. A miscut of the substrate introduces surface steps in a regular distance: For 2° miscut the regular spacing of steps can be calculated to approximately 11 nm. As shown in figure 7(c), the average domain size is significantly larger than the regular spacing of the surface steps indicating that domain

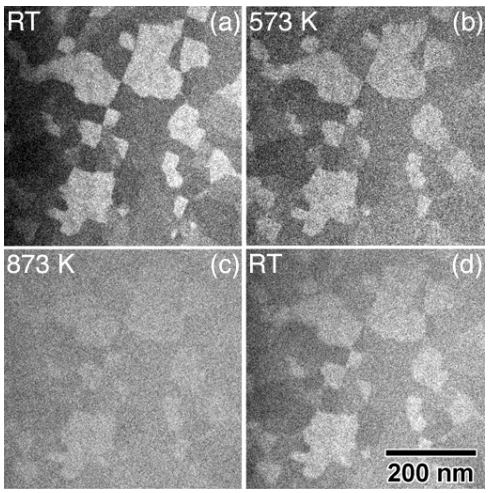

Figure 8. Dark-field TEM image of LFO thin film grown on (001) STO taken at (a) RT, (b) 573 K, (c) 873 K and (d) after cooling to RT.

structures overgrow the step edges. On a miscut substrate, the initial nucleation of the first unit cells preferentially takes place at the step edges as the deposited material diffuses and accumulates there, forming elongated chains along the step edges. Therefore, a long-range periodicity of the *c*-axis can readily be established along the step edges whereas the *c*-axis orientation perpendicular to the step edges is hampered.

In order to find out the thermal stability of the structural domains, *in situ* heating experiment was carried out inside a TEM (figures 8(a)–(c)). A gradual reduction of the domain contrast was observed but the domain shape clearly remained. The weakening of the contrast is somewhat correlated with thermal vibration or with contamination of the sample due to the poor vacuum in the TEM. However, since the domain contrast recovered upon cooling (figure 8(d)), it is evident that the contrast weakening is mainly correlated with the intensity decay of the 001 reflection of LFO. This result corroborates the RHEED observation [13] that the relative intensity of the additional streak increases almost linearly upon cooling (see figure 4(c)).

LFO is an orthoferrite with a strong tendency towards twin formation. As reported by Marezio and Dernier [18], structural twins also exist in the bulk phase of LFO. Although the orthorhombicity of LFO is small, the lattice is very rigid to deform into a tetragonal or cubic unit cell, even when grown on a cubic substrate with a small lattice mismatch. We tried to grow LFO coherently with the substrate; the thinnest film (2 nm), which contained 4 unit cells of LFO, already consisted of structural domains. This observation is consistent with the RHEED patterns obtained during the initial stage of growth (see figure 4); the additional streaks of LFO appear as soon as the deposition starts indicating that the symmetry of LFO becomes lower compared to cubic STO already in the first unit cell. Thus, we assume that LFO grows at 750 °C from the initial state in a tetragonal or orthorhombic state. This is consistent with the observation of Marezio and Dernier that the LFO bulk crystals do not grow as cubic from melts [18].

Basically, the orthorhombicity of LFO is given by the buckling angle of the Fe–O–Fe bonding (see figure 1(b)). The fact that the domain shape is preserved during the heating experiment suggests that the buckling angle remains the same within a domain. In addition, the decrease of both, the domain contrast and the relative RHEED intensity, imply that the buckling angle increases with the temperature towards 180 °C.

5. AFM properties of LFO thin films

The recent developments of synchrotron radiation-based PEEM have enabled the imaging of AFM domains in LFO thin films [8]. Linear x-ray polarization was used to image the AFM domain structure in LFO films, making use of the large XMLD effect associated with the multiplet structure at the Fe L_3 or L_3 edge [8]. Details about the PEEM measurements can be found in [12, 23]. To summarize, the PEEM-2 microscope at the ALS used linearly polarized x-rays incident on the sample at an angle of 30° from the surface and with the electric field vector $\vec{E}$ oriented parallel to the film surface. The XMLD effect depends on the angle θ between the x-ray polarization and the AFM axis $\vec{A}$ as well as on the expectation value of the square of the magnetic moment $\langle M^2 \rangle_T$. Thus, AFM domains appear bright and dark in the PEEM image (see figure 9 taken at 290 K) depending on their $\vec{A}$ axis, and their contrast scales with the temperature proportional to $\langle M^2 \rangle_T$ (figure 9).

In figure 10(a) AFM domains of LFO grown on (001) STO are shown. Below the PEEM image, XMLD spectra recorded in the bright and dark domain regions reveal the spectroscopic origin of the AFM contrast: the bright region gives rise to enhanced second peaks of the Fe L_3 and L_2 edges whereas in the dark region the first peaks are larger. In practice, a PEEM image was acquired for instance at 723.2 eV at the second peak of the Fe L_2 edge and divided by one obtained at the first peak of the Fe L_2 edge at 721.5 eV. From a detailed study of the angular dependence of the XMLD effect in LFO films, the AFM axis was found to be inclined 45° from the surface normal and to be parallel or perpendicular to the $\vec{E}$ vector [12]. In figure 10(a), the projection of the x-ray propagation direction is parallel to the vertical axis of the image, thus, the $\vec{E}$ vector lies parallel to the film surface and parallel to the vertical axis of the image. The in-plane orientations of the AFM axis are schematically indicated in the inset.

The comparison of PEEM and TEM results [8, 12, 13] as well as PEEM and SEM [19] have revealed that the structural domains in LFO thin films are directly correlated with AFM domains. LFO is an orthoferrite with a strong spin–lattice interaction, which is correlated with the Fe–O–Fe bonding. The latter controls on the one hand the orthorhombicity of LFO via the buckling angle and on the other hand the AFM ordering via superexchange coupling of Fe-ions. Also by considering the bulk symmetry *Pbnm* of LFO, it is clear that the crystallographic orientation confines the spin orientations in LFO yielding the direct correlation between structural and AFM domains [8, 12, 13].

By collecting XMLD images obtained at different temperatures the Néel temperature T_N was determined to 670 ± 10 K, which is lower compared to that of bulk LFO with $T_N = 740$ K [8]. As can be seen in figure 9, the XMLD contrast is strongly reduced at elevated temperatures and it is

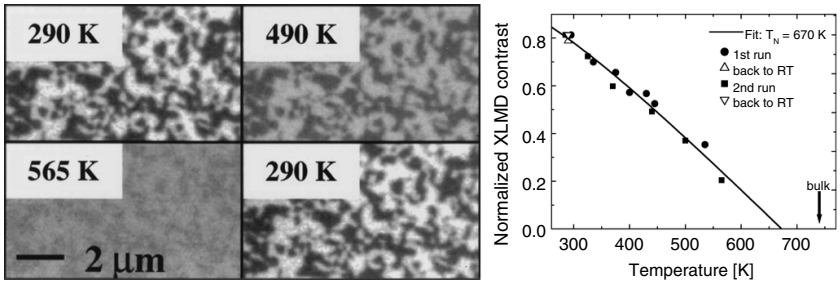

Figure 9. XMLD images recorded at four different substrate temperatures for the LFO thin films on (001) STO. Temperature dependence of the XMLD contrast is plotted with a fit (solid line) to $\langle M^2 \rangle$ from mean field theory. The fit gives an estimate for the Néel temperature of 670 K. From [8]. Reprinted with permission from AAAS.

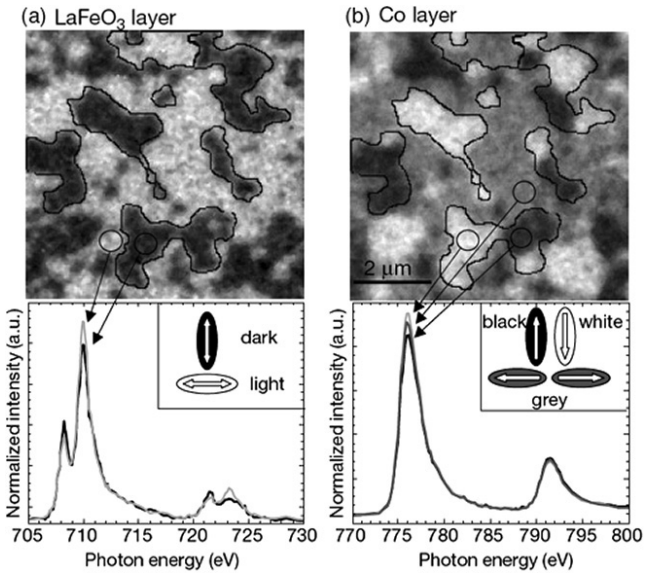

Figure 10. (a) Fe L-edge XMLD and (b) Co L-edge XMCD image and the local spectra recorded from the indicated areas in the antiferromagnetic LFO and the ferromagnetic Co thin films grown on (001) STO [9]. The contrast in the XMLD image arises from AFM domains in LFO with in-plane orientations of the AFM axis parallel (light) and perpendicular (dark) to the horizontal $\vec{E}$ vector, as indicated below the image. The contrast in the XMCD image contains three distinct gray scales, corresponding to FM domains with spins aligned antiparallel (black), parallel (white) or orthogonal (gray) to the x-ray propagation direction. Detailed description can be found in the text. Reprinted by permission from Macmillan Publishers Ltd: Nature [9], copyright (2000).

completely reversible upon cooling to room temperature. The AFM domain shape is preserved upon heating and cooling indicating that the domain boundary remain fixed. This finding clearly supports the direct correlation between crystallographic and the AFM domains. Nevertheless, AFM domains are stable up to Néel temperature whereas structural domains exist at higher temperatures. Grepstad *et al* have recently reported that the size of crystallographic domains increases upon annealing at 1000 °C in oxygen [20]. This finding combined with our RHEED observations suggests that the structural transition occurs below 1000 °C but above 750 °C.

The reduced Néel temperature has been attributed to epitaxial strain, which affects exchange coupling constant J through changes in the Fe–O–Fe superexchange angle. As measured by XRD and TEM, LFO unit cell suffers an out-of-plane expansion of about 0.4% and an in-plane contraction and expansion of about 0.2% along and perpendicular to the c-axis, respectively. In total, the LFO unit cell volume increases leading to an increased Fe–O–Fe bonding distance weakening the superexchange between Fe atoms and thus reducing the Néel temperature. Recently, Grepstad *et al* have reported that relaxed LFO thin films, obtained after a thermal annealing in oxygen at 1000 °C, also revealed a low T_N indicating that epitaxial strain cannot be the reason for the T_N reduction [20]. Moreover, they found that crystallographic domains as well as AFM domains become larger and that the AFM axis changes its orientation upon annealing. XMLD spectroscopy [12] and microscopy studies [21] have also revealed that the AFM axis in LFO thin films differs from that of bulk. Since within the *Pbnm* space group the orientation of the AFM axis is strongly restricted due to symmetry considerations, one has to conclude that the crystal symmetry in these thin films may slightly differ from that of bulk LFO. A deviation of the AFM axis from the ideal bulk direction, and therefore a change in crystal symmetry, has also been observed for polycrystalline LFO [22]. As illustrated in figure 2, in orthoferrites T_N scales with the buckling angle α. As T_N decreases in thin films, it may be that α in thin films is reduced compared to that in bulk LFO.

6. Exchange bias in Co/LFO and Fe/LFO thin films

In order to study the exchange bias in LFO layers, a thin film of Fe or Co was deposited *in situ* at room temperature and capped with a 1 nm Pt layer to prevent its oxidation. XRD and TEM analysis revealed a polycrystalline Fe and Co structure. Kerr measurements showed that the easy magnetization axis of the sample was in-plane with uniaxial symmetry about the surface normal. For the PEEM experiments, only Co layers were used. As the probing depth of PEEM using low-energy secondary electrons is in the range of 2–5 nm, LFO and Co layers can be imaged at the same time. The elemental specificity of x-ray absorption techniques allows distinguishing both layers, by acquiring images at the characteristic absorption resonances (Fe L-edge near 710 eV and Co L-edge near 780 eV). In addition, by exploiting the polarization dependence of x-ray absorption in magnetic materials, AFM domains of

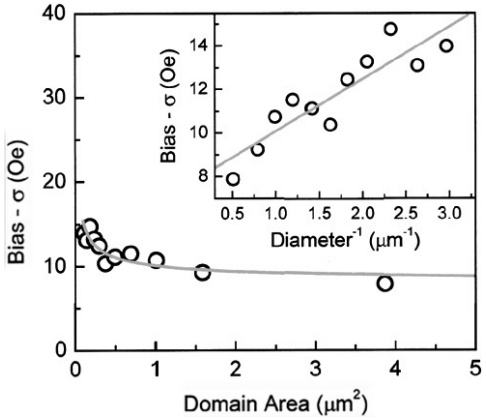

Figure 11. Exchange bias field distribution as a function of domain area determined from microscopic maps domain by domain. Inset shows the same data as a function of inverse domain diameter. The lines are fit with a linear function of the inverse domain diameter. Reused with permission from [10]. Copyright 2004, American Institute of Physics.

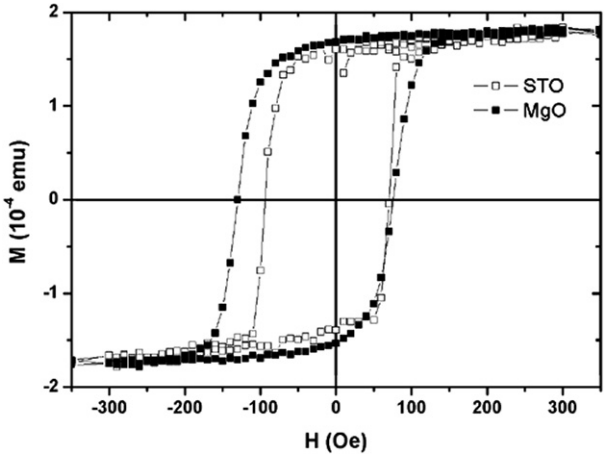

Figure 12. $M(H)$ measurement of the LFO/Co thin films grown on STO and MgO with exchange bias field of 12 Oe and 37 Oe, respectively.

LFO can be imaged using XMLD whereas the ferromagnetic domains in Co can be studied using x-ray magnetic circular dichroism (XMCD). A detailed description of the experimental procedures can be found in [9, 23].

Figure 10 shows representative images of the domain structure in the AFM LFO film and in the FM Co layer directly on top. As already described in section 5, the magnetic contrast in LFO arises from AFM domains with an in-plane projection of the AFM axis oriented parallel (light) and perpendicular (dark) to the horizontal electrical field vector $\vec{E}$, which is parallel to the film surface and the vertical axis of the image. The Co XMCD images were obtained by using circular polarized x-ray with the photon angular momentum oriented parallel to the x-ray propagation direction, at a 30° angle from the surface. The FM Co image in figure 10(b) exhibits three distinct gray scales, corresponding to FM domains with in-plane spin orientation aligned vertically up (black) and down (white), and horizontally left or right (gray). XMCD spectra, shown below the image, recorded for regions with different gray scales illustrate the origin of the intensity contrast: the intensity ratio of the peaks at the Co L_3 edge and at the Co L_2 edge depends on the orientation of the magnetic moment. Hence, XMCD images were obtained by dividing images acquired at these edges. As the projection of the x-ray propagation direction, as well as that of the angular momentum, is directed vertically down in-plane, we can conclude that Co domains appear white or black as their spins are parallel or antiparallel to the beam direction. Domains with spins pointing to the left and the right, orthogonal to the beam direction, appear in the same gray shade and are not differentiated in this image. Comparison of these images clearly illustrates that the FM Co spins are aligned parallel or antiparallel to the in-plane projection of the AFM axis of LFO indicating that the alignment of the FM spins is coupled, domain by domain, by the spin directions in the underlying antiferromagnetic layer [9]. This correlation is clearly of magnetic origin rather than crystallographic origin as the Co is polycrystalline and no preferential structural correlation could be found by TEM and XRD.

These PEEM measurements were performed on as-grown samples, i.e. they were not set in a magnetic field above the Néel temperature and field-cooled. Therefore they did not exhibit a macroscopic exchange bias. However, local exchange bias could be observed when the magnetic field dependence of the magnetization direction of the Co domains was studied by taking XMCD images after applying magnetic field pulses [9, 10]. The field was applied along the in-plane projection of the x-ray propagation and the images were acquired in zero field. From the field dependent XMCD contrast in a series of images, microscopic maps of the exchange bias field domain by domain were constructed. The bias field distribution as a function of the domain size is shown in figure 11. A significant increase of the bias field distribution can be seen with decreasing domain size, which clearly scales with the inverse domain diameter $\sim 1/d$ [10].

Correlations between exchange bias and pinned magnetization in the AFM has been observed for instance in an XMCD study [6] and in a magneto-optic Kerr effect study [24]. In particular, a polarized neutron reflectometry study of exchange biased Co/LFO revealed that the antiferromagnet develops a net moment only close to the interface [25]. In a polycrystalline AFM, the number of interfacial uncompensated spins were found to inversely scale with the grain size [4]. Our attempts to image directly the uncompensated Fe spins on the LFO surface with XMCD microscopy were unsuccessful, probably because of their small concentration.

Macroscopic magnetic characterization of the samples was performed with a VSM and a SQUID magnetometer. Figure 12 shows the VSM measurements carried out at room temperature for LFO/Co bilayers grown on (001) MgO and (001) STO. Both films were grown under comparable conditions and were set in a magnet field of 5000 Oe at 120 °C for 15 min. The observed exchange bias is about three times higher for the sample grown on MgO than that on STO.

The exchange bias shift obtained by using LFO thin films was generally in the range of 10–40 Oe. Such a low

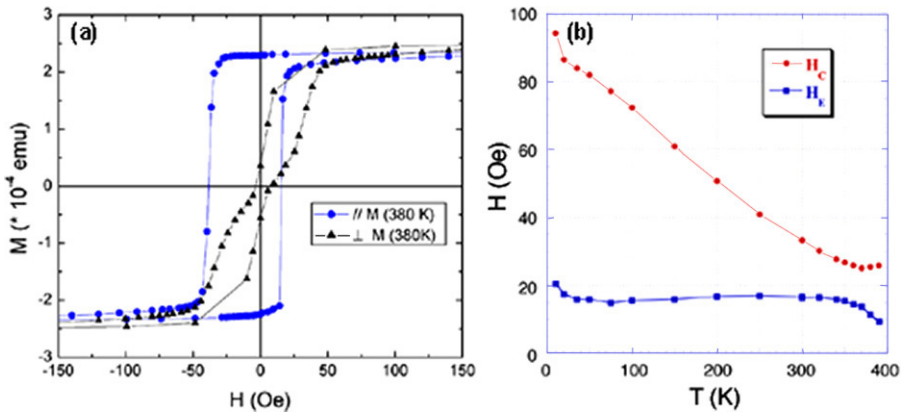

Figure 13. (a) $M(H)$ loops of LFO/Fe grown on (001) MAO substrate, measured at $T = 380$ K parallel and perpendicular to the setting field direction. The LFO and Fe thickness correspond to 30 nm and 8 nm, respectively. (b) Temperature dependence of the exchange bias field H_E and coercive field H_C.

macroscopic exchange bias shift might be explained by the fact that the samples have only been set at 120 or 200 °C, i.e. far below the Néel temperature. It has to be stated that field cooling through the high Néel temperature of 740 K was impossible. Annealing to T_N would result in chemical decomposition and/or interdiffusion between the LFO and the FM Co or Fe layers. It has been reported that exchange bias can be established below the T_N [26], however, the full biasing potential of the LFO could not be achieved.

Clearly higher exchange bias field was obtained for the films grown on MgO and MAO than that on STO and LAO. As TEM analysis revealed (see section 4), LFO films grown on MgO and MAO substrates contained significantly smaller structural domains compared to that in the films grown on STO and LAO. Unfortunately, their average diameter has been below the actual resolution limit of the PEEM technique in order to determine the size of the AFM domains and to measure the local bias field domain by domain. Figure 13(a) shows hysteresis loops of a LFO/Fe film grown on (001) MAO substrate with a thickness of 30 nm and 8 nm, respectively, measured at $T = 380$ K parallel and perpendicular to the setting field direction. The temperature dependence of the exchange bias field presented in figure 13(b) reveals that the exchange bias field remains almost constant around 16 Oe in the temperature range of 325 K down to 50 K and slightly rises to 22 Oe by cooling down to 10 K. The coercive field H_C increases linearly with the cooling temperature up to 94 Oe at 10 K.

Taking into account that the structural domains are directly correlated with AFM domains, we can conclude that the macroscopic exchange bias inversely scales with the domain size in agreement with the findings of exchange bias field on the microscopic scale [10]. However, for the samples grown on STO the macroscopic exchange bias shift was in the range of about 10 Oe and, surprisingly, neither the LFO film thickness nor the substrate orientation had a significant effect on the macroscopic shift, although our TEM [17] and PEEM [12] experiments clearly revealed a domain size dependence on these parameters.

In LFO thin films grown on MgO and MAO substrates, the difference in domain size and domain configuration might originate from the lattice mismatch between the film and the substrate. With a lattice mismatch of about 6.7% and 3%, respectively, it is very likely that more domains nucleate on MgO or MAO substrates, as domain walls generally lead to strain relaxation. Moreover, on MgO and MAO the third domain type with the *c*-axis out-of-plane occupies about one third of the total film surface. Although we do not rule out that the reduced domain size is indeed the major parameter responsible for the exchange bias, we strongly assume the domain wall configuration also plays an important role. As described in detail in [17], 90° rotational twins typically form straight and well-defined domain boundaries with facets parallel to the *c*-axis whereas the third domain type yields curved and poorly defined boundaries. Thus, one could speculate that ill-defined, curved domain boundaries may give rise to more pinned uncompensated spins than well defined and straight ones.

7. Diluted $La(Ni_{0.1}, Fe_{0.9})O_3$ in exchange bias

Implementation of nonmagnetic defects in the AFM has proven to affect the formation of the AFM domains and to influence exchange bias [27–29]. We have diluted the volume part of the AFM by substitution of about 10% of Fe by Ni. On top of this diluted LNFO layer, a three unit cell thin layer of LFO was deposited in order to ensure that the dilution has only an influence on the generated domain structure and not on the chemical or magnetic state of the AFM/FM interface. Inset of figure 14 shows schematically the layer structure of the sample. The temperature dependence of the exchange bias field of the Co/LFO/LNFO system grown on STO substrate is presented in figure 14, in comparison with Co/LFO systems grown on various substrate materials. A significant difference between the samples is found at low temperatures: Below 180 K the exchange bias field increases exponentially for the sample containing the diluted AFM whereas it remains almost constant for the non-diluted samples. Up to now, it is unclear why the bias sets in at 180 K. One could suggest that the

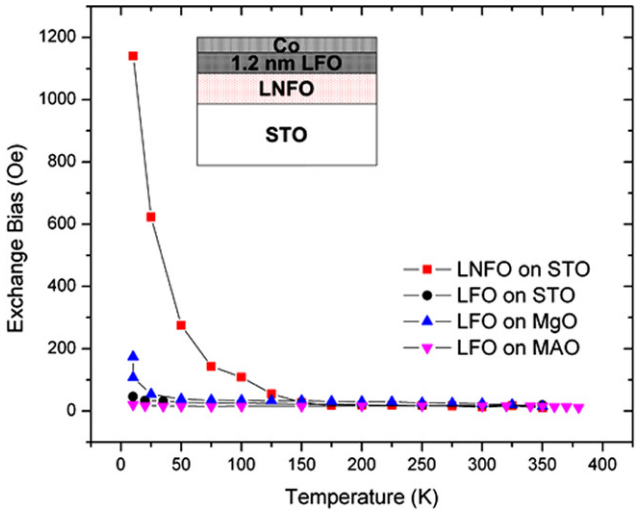

Figure 14. The temperature dependence of the exchange bias field of the sample containing the LNFO diluted layer in the volume part compared to those grown on STO, MgO, and MAO substrates.

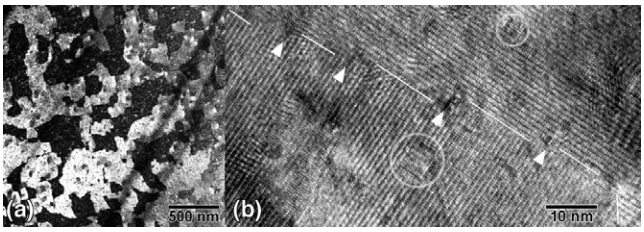

Figure 15. (a) Dark-field TEM image of LFO/LNFO thin film grown on (001) STO. (b) HRTEM image indicates a grain boundary with short segments of about 10 nm. Between two segments (marked by white arrow heads) dark contrast appears indicating local strain field. White circles indicate small domains with a diameter less than 10 nm.

Néel temperature is significantly lowered due to the modified domain structure caused by the diluted LNFO in the volume part. As a consequence, the setting temperature might be now much closer to T_N, leading to a much better coupling between the Co and the uncompensated spins in the AFM.

Enhancement of exchange bias with diluted antiferromagnets have mainly been studied by substitution of nonmagnetic impurities [27, 28]. For instance Miltenyi *et al* have shown in diluted CoO systems ($Co_{1-x}Mg_xO$ and Co_yO) that the substitutional defects increase the exchange bias field by a factor of 2–3 at 5 K [27]. Hong *et al* [28] observed an enhancement by a factor of four at 10 K. In our LNFO system, an increase of a factor of 10 was obtained at 5 K.

A diluted AFM in an external magnetic field develops a domain state when cooled below its Néel temperature [27]. Defects substantially favor the formation of domains in the diluted AFM, in particular, the domain walls pass preferentially through nonmagnetic defects at no cost of exchange energy [30]. In the present system, by substituting Ni atoms into the AFM LFO layer $LaNiO_3$ sites are created in the LFO matrix. $LaNiO_3$ is paramagnetic in its bulk phase and nearly cubic with a lattice parameter of 3.84 Å at room temperature. Hence, Ni substitution leads to structural defects with local strain fields strongly governed by the lattice mismatch of about 2.5%. The strain field caused by the substitutional defects can be minimized if the domain walls pass preferentially through structural defect sites.

Figure 15(a) shows a dark-field plan-view image of the LFO/LNFO sample. Domains with an average size of 200 nm can be seen, similar to films without diluted LFO. However, the domain shape is strongly irregular and the domain size distribution is broad. Energy dispersive x-ray analysis showed that the Ni atoms were distributed homogeneously within the LFO film without any indication of second phase formation or segregation to grain boundaries. In contrast to the domain images in figures 5(b) and 7, tiny bright and dark dots appeared, which became most well visible by tilting the sample out of the zone axis. They are preferentially present at domain boundaries with a spacing of about 10–20 nm, but also within large domains.

In HRTEM (figure 15(b)), it can be seen that the domain boundary consists of short straight sections (about 10 nm). Between two sections dark contrast is visible (marked by white arrow heads). We assume that at these locations substitutional defects are present and initiates the boundary to run through these defects. The dark contrast might originate from the local strain field around the defect itself as well as the joining of two segments. As a consequence, compared to the boundary present in pure LFO films (figures 5(b) and 7) the domain boundary is curved and poorly aligned. Moreover, presence of small domains with a diameter less than 10 nm can be observed as marked by white circles. These inclusions correspond to the tiny bright and dark dots observed in the dark-field TEM image. By means of fast-Fourier-transformation, we could verify that these are indeed small domains with the other twin configuration. In a few cases, the third domain configuration, which was present in the sample grown on MgO and MAO, could be detected. Hence, the dilution does not only change the shape of the domain boundary because domain boundaries preferentially pass the statistical defect sites but also stabilizes formation of additional small domains within a large domain, enabling even orientations which were not present in the non-diluted case.

One has to keep in mind that diluting the AFM layer occurs in the volume part away from the FM/AFM interface. Hence, the LNFO layer is not in direct contact with the magnetic Co layer. Therefore we can exclude that substitutional defects or the magnetic moment of Ni atoms have a direct influence on the LFO/Co interface. The dilution rather supports the formation of volume domains in the non-diluted AFM. Owing to the direct correlation between the structural and AFM domains in LFO, it is likely that the superexchange coupling will be interrupted at domain boundaries and lead to uncompensated spins. As already discussed, smaller domains lead to higher exchange bias field in agreement with the random-field model of Malozemoff [3] and with the experimental data and their interpretation by Takano [4]. Thus, the domain inclusions as observed in figure 15 will lead to a higher number of

uncompensated spins. However, our results also suggest that a poorly defined domain boundary may result in a higher number of uncompensated spins. This might explain our findings that 90° rotational twins with a low-indexed habit plane as present in LFO grown on STO substrates lead to a small negligible net moment although the domain size and shape can significantly be changed by varying the film thickness, the orientation and the miscut of the substrate.

Our result may hint the direct correlation between exchange bias and the presence of uncompensated spins located at inhomogeneities (defects, impurities, domain boundaries etc), which break the translational symmetry of the crystal, in agreement with Ghadimi *et al* [29]. Depending on the degree of symmetry breaking, some spins might strongly be anchored in the AFM and appear as pinned uncompensated moment. Considering the result of Hoffmann *et al* [25], it is also possible that the uncompensated spins at domain boundaries in the top most part of LFO alter due to surface relaxation and due to the coupling to a ferromagnet and lead to an enhanced net moment at the interface compared to the volume part.

8. Conclusion

We have reviewed the growth, structural and AFM properties, and exchange coupling of LFO thin films to adjacent FM layer. We demonstrated that the structural domain configuration in LFO can change with the substrate material, orientation and its miscut. In LFO, due to the Fe–O–Fe superexchange, which determines the AFM properties as well as the orthorhombicity of the unit cell, structural domains are directly correlated with AFM domains. Consequently, exchange bias can be modified by changing the structural domain configuration. The highest exchange bias field was obtained in the films grown on MgO and MAO where the smallest domains have been found, in agreement with the recent PEEM result [10]. However, our results also indicate that the domain boundary configuration at the atomic scale also plays an important role to the resulting exchange bias field. In addition, a ten-fold increase of exchange bias was obtained by diluting LFO in the volume part. In this film, the domain boundary was found to cross the substitutional defects and become irregular. Considering the Fe–O–Fe bonding configurations, we speculate that a poor bonding alignment at an irregular domain boundary may yield uncompensated spins.

Acknowledgments

We acknowledge stimulating discussion with Ch Dieker, H Siegwart, J Lüning, S Raoux, J Stöhr, T Ramsvik, A Hoffmann and I K Schuller. Authors also thank the Centre Interdisciplinaire de Microscopie Electronique at the EPFL for access to electron microscopes.

References

[1] Nogues J and Schuller I K 1999 *J. Magn. Magn. Mater.* **192** 203
[2] Mauri D, Siegmann H C, Bagus P S and Kay E 1987 *J. Appl. Phys.* **62** 3047
[3] Malozemoff A P 1988 *J. Appl. Phys.* **63** 3874
[4] Takano K, Kodama R H, Berkowitz A E, Cao W and Thomas G 1997 *Phys. Rev. Lett.* **79** 1130
[5] Takano K, Kodama R H, Berkowitz A E, Cao W and Thomas G 1998 *J. Appl. Phys.* **83** 6888
[6] Ohldag H, Scholl A, Nolting F, Arenholz E, Maat S, Youn A T, Carey M and Stöhr J 2003 *Phys. Rev. Lett.* **91** 17203
[7] Kappenberger P, Martin S, Pellmont Y, Hug H J, Kortright J B, Hellwig O and Fullerton E E 2003 *Phys. Rev. Lett.* **91** 267202
[8] Scholl A, Stöhr J, Lüning J, Seo J W, Fompeyrine J, Siegwart H, Locquet J P, Nolting F, Anders S, Fullerton E E, Scheinfein M R and Padmore H A 2000 *Science* **287** 1014
[9] Nolting F, Scholl A, Stöhr J, Seo J W, Fompeyrine J, Siegwart H, Locquet J P, Anders S, Lüning J, Fullerton E E, Toney M F, Scheinfein M R and Padmore H A 2000 *Nature* **405** 767
[10] Scholl A, Nolting F, Seo J W, Ohldag H, Stöhr J, Raoux S, Locquet J P and Fompeyrine J 2004 *Appl. Phys. Lett.* **85** 4085
[11] Lyubutin I S, Dmitrieva T V and Stepin A S 1999 *J. Exp. Theor. Phys.* **88** 590
[12] Lüning J, Nolting F, Scholl A, Ohldag H, Seo J W, Fompeyrine J, Locquet J P and Stöhr J 2003 *Phys. Rev.* B **67** 214433
[13] Seo J W, Fompeyrine J, Siegwart H and Locquet J P 2001 *Mater. Res. Soc. Symp. Proc.* **666** F8.8.1
[14] Locquet J P, Catana A, Mächler E, Gerber Ch and Bednorz J G 1994 *Appl. Phys. Lett.* **64** 372
[15] Marezio M, Remeika J P and Dernier P D 1970 *Acta Crystallogr.* B **26** 2008
[16] Boekema C, Van der Woude F and Sawatzky G A 1972 *Int. J. Magn.* **3** 341
[17] Seo J W, Fompeyrine J, Siegwart H and Locquet J P 2006 *Int. J. Mater. Res.* **7** 943
[18] Marezio M and Dernier P D 1971 *Mater. Res. Bull.* **6** 23
[19] Czekaj S, Nolting F, Heydermann L J, Kunze K and Krüger M 2007 *J. Phys.: Condens. Matter* **19** 386214
[20] Grepstad J K, Takamura Y, Scholl A, Hole I, Suzuki Y and Tybell T 2005 *Thin Solid Films* **486** 108
[21] Czekaj S, Nolting F, Heydermann L J, Willmott P R and van der Laan G 2006 *Phys. Rev.* B **73** 020401(R)
[22] Peterlin-Neumaier T and Steichele E 1986 *J. Magn. Magn. Mater.* **59** 351
[23] Scholl A, Nolting F, Stöhr J, Lüning J, Seo J W, Locquet J P, Fompeyrine J, Anders S, Ohldag H and Padmore H A 2001 *J. Synchrotron. Radiat.* **8** 101
[24] Sampaio L C, Mougin A, Ferré J, Georges P, Brun A, Bernas H, Poppe S, Mewes T, Fassbender J and Hillebrands B 2003 *Eur. Phys. Lett.* **64** 819
[25] Hoffmann A, Seo J W, Fitzsimmons M R, Siegwart H, Fompeyrine J, Locquet J P, Dura J A and Majkrzak C F 2002 *Phys. Rev.* B **66** 220406
[26] Berkowitz A E, Hansen M F, Kodama R H, Tang Y J, Hong J I and Smith D J 2005 *Phys. Rev.* B **72** 134428
[27] Miltenyi P, Gierlings M, Keller J, Beschoten B, Güntherodt G, Nowak U and Usadel K D 2000 *Phys. Rev. Lett.* **84** 4224
[28] Hong J I, Leo T, Smith D J and Berkowitz A E 2006 *Phys. Rev. Lett.* **96** 117204
[29] Ghadimi M R, Beschoten B and Güntherodt G 2005 *Appl. Phys. Lett.* **87** 261903
[30] Esser J, Kowak U and Usadel K S 1997 *Phys. Rev.* B **55** 5866